Supported Phospholipid Bilayers Prepared by the "LB/Vesicle Method": A Fourier Transform Infrared Attenuated Total Reflection Spectroscopic Study on Structure and Stability

Peter Wenzl,[†,§] Marianna Fringeli,[‡] Jeannette Goette,[‡] and Urs Peter Fringeli*[,†,‡]

Institute for Physical Chemistry, University of Vienna, P.O. Box 217, A-1091 Vienna, Austria, and ETH-Technopark, Pfingstweidstrasse 30, CH-8005 Zürich, Switzerland

Received June 13, 1994[⊗]

The purpose of this study is to present a reliable and easy method for the preparation of supported phospholipid bilayers which consists of two steps: (1) transfer of a Langmuir–Blodgett (LB) monolayer onto a solid substrate and (2) completion of the bilayer by adsorption of phospholipid molecules from a vesicle solution. Two types of asymmetric bilayers have been prepared, a DPPA/POPC bilayer with the DPPA leaflet in the gel and the POPC leaflet in the liquid crystalline phase, and a DPPA/DPPC bilayer with both leaflets in the gel phase. The method may be applied for the preparation of symmetric bilayers as well. The surface concentration, Γ, the molecular area A_{mol}, and the mean molecular order parameter $\bar{S}_{mol}$ of the hydrocarbon chains were determined for each leaflet of the resulting bilayers separately by means of quantitative FTIR-ATR spectroscopy (Fourier transform infrared attenuated total reflection spectroscopy). An orientational model which also takes into account a hydrocarbon chain tilt in the gel phase was employed to derive $\bar{S}_{mol}$. Values obtained for A_{mol} and $\bar{S}_{mol}$ in different leaflets coincide with the values for the respective phospholipids given in the literature. The stability of the immobilized LB-DPPA monolayer and the two different supported bilayers in an aqueous environment was monitored over a period of at least 60 h. Possible mechanisms of bilayer formation during preparation are discussed. Finally, the usefulness of these bilayers for quantitative in situ FTIR-ATR studies on the interaction of such model membranes with substrates dissolved in the aqueous environment is stressed.

Introduction

It has been shown in a series of papers that organized monolayer assemblies can be prepared on various surfaces by controlling processes of molecular self-organization of lipidlike molecules, e.g. via transferring Langmuir–Blodgett (LB) monolayers or direct adsorption.[1-6] Well-ordered bilayer assemblies adsorbed to a solid substrate ("supported bilayers") are more difficult to obtain. But they are of great interest from biophysical, biochemical, and biomedical viewpoints. Tamm and McConnell reported a procedure for the preparation of the second leaflet of a supported bilayer. They placed a solid substrate, which had already been coated with a LB monolayer, onto another LB monolayer at the air–water interface and pushed it through the interface into the subphase.[7] In this article we report a different technique which has been used in our laboratory for several years.[8-13] Recently, mixed POPC/POPG bilayers have been prepared by this technique for mellitin orientation studies.[14] The proposed preparation procedure (see below) has also been successfully used for the preparation of a supported thiolipid/DMPC bilayer.[15]

The preparation presented in this paper consists of two independent steps. The first leaflet of the bilayer is transferred as a compact monolayer by the well-known LB technique onto a solid substrate (ATR plate) with the polar head groups in contact with the solid support. In the second step, a vesicle solution is contacted slowly and in a controlled manner with the immobilized monolayer. Due to the thermodynamically unfavorable state of the hydrophobic surface of the immobilized first leaflet, lipid molecules of the vesicle solution adsorb spontaneously to this leaflet, thereby building up the second leaflet of the supported bilayer.

We have used 1,2-dipalmitoyl-*sn*-glycero-3-phosphoric acid (DPPA) for the first leaflet of the supported bilayer and 1-palmitoyl-2-oleoyl-*sn*-glycero-3-phosphocholine (POPC) as well as 1,2-dipalmitoyl-*sn*-glycero-3-phosphocholine (DPPC) for the second leaflet. At 25 °C, both leaflets of the DPPA/DPPC bilayer were in the gel phase (DPPA, L_{β}; DPPC, $L_{\beta'}$), while the POPC leaflet of the DPPA/POPC bilayer was in the liquid crystalline phase (L_{α}).

The scientific motivation for our research was predominantly the development of a reproducible method for the preparation of stable immobilized bilayer membranes, which can be used for in situ drug-membrane interaction studies. The combination with IR-ATR techniques not only enables in situ monitoring of bilayer formation but also results in direct access to membrane–water partition coefficients as well as to molecular structures and structural changes of drug and membrane upon interaction.

* Author to whom correspondence should be addressed.
† University of Vienna.
‡ ETH-Technopark.
§ Present address: Biotechnology Research Unit, CIAT, Apartado Aéreo 6713, Cali, Colombia.

⊗ Abstract published in *Advance ACS Abstracts,* October 15, 1994.

(1) Blodgett, K. B. *J. Am. Chem. Soc.* **1935**, *57*, 1007.
(2) Blodgett, K. B.; Langmuir, I. *Phys. Rev.* **1937**, *51*, 964.
(3) Higashiyama, T.; Takenaka, T. *J. Phys. Chem.* **1974**, *78*, 941.
(4) Maoz, R.; Sagiv, J. *J. Colloid Interface Sci.* **1984**, *100*, 465.
(5) Sugi, M. *J. Mol. Electron.* **1985**, *1*, 3.
(6) Ohtake, T.; Mino, N.; Ogawa, K. *Langmuir* **1992**, *8*, 2081.
(7) Tamm, L. K.; McConnell, H. M. *Biophys. J.* **1985**, *47*, 105–113.
(8) Schöpflin, M.; Fringeli, U. P.; Perlia, X. *J. Am. Chem. Soc.* **1987**, *109*, 2375.
(9) Fringeli, U. P. In *Biologically Active Molecules*; Schlunegger, U. P., Ed.; Springer: Berlin, 1989; p 241.
(10) Fringeli, U. P.; Apell, H. J.; Fringeli, M.; Läuger, P. *Biochim. Biophys. Acta* **1989**, *984*, 301.
(11) Fringeli, U. P. *Chimia* **1992**, *46*, 200.
(12) Fringeli, U. P. In *Internal Reflection Spectroscopy*; Mirabella, F. M., Ed.; Marcel Dekker: New York, 1992; p 255.
(13) Goette, J. Ph.D. Thesis No. 9721, ETH-Zürich, 1992.
(14) Frey, S.; Tamm, L. K. *Biophys. J.* **1991**, *60*, 922.
(15) Lang, H.; Duschl, C.; Grätzel, M.; Vogel, H. *Thin Solid Films* **1992**, *210/211*, 818.

0743-7463/94/2410-4253$04.50/0

Experimental Section

1. Materials. DPPA was purchased from R. Berchtold (Biochemisches Laboratorium, Berne), DPPC from Fluka AG, and POPC from Sigma. Chemicals were used without further purification. Water was triply distilled; a potassium permanganate stage was first used to oxidize organic impurities, followed by a double quartz distillation. In all experiments, the same phosphate buffer (20 mM Na_2HPO_4/NaH_2PO_4, pH = 7.0, 100 mM NaCl, and 0.1 mM $CaCl_2$) was used. The subphase in the LB trough was a 0.1 mM $CaCl_2$ solution. All glassware was rinsed with a $Na_2Cr_2O_7$ solution and washed several times with deionized water, triply distilled water, and ethanol prior to use.

2. SBSR Attachment. The ATR plate applied for all experiments was a 52 × 30 × 2 mm^3 germanium trapezoid. An angle of incidence $\theta = 45°$ resulted in 25 internal reflections. With the help of a computer-controlled chopper, the IR beam was passed alternatively through the *sample* (S) in the lower part, and the *reference* (R) in the upper part of the ATR plate. As S and R can be measured with a single beam without cell displacement, this technique is referred to as the *single-beam-sample-reference* (SBSR) method.[9] The corresponding spectra, i.e. S/R and −log(S/R), are called SBSR transmittance and absorbance spectra, respectively.

A self-constructed SBSR cell made of Delrin was used. The S and R compartment consisted of two cuvettes on both sides of the ATR plate, respectively. The outlet of the cuvette on one side was connected in series to the inlet of the opposite cuvette. Viton O-rings were used to seal the S and the R cuvettes, pressing the SBSR cell body against the ATR plate. The cuvettes have been hydrodynamically optimized with respect to flow-through experiments, featuring a rectangular shape (30.6 × 12.5 mm^2), terminated on either side by a half circle (r = 6.25 mm). For the IR beam this configuration resulted in a mean length of the ATR plate which was in contact with the solution-filled cuvettes of 38.6 mm. This corresponded to a mean number of solution sensing internal reflections (N_{aq}) of 19.3. The distance between the ATR plate and cell body was ~150 μm, resulting in a volume of ~75 μL per cuvette. Temperature regulation of the SBSR cell within ±0.2 °C was achieved by an external thermostat with circulating water. The temperature of the cell was monitored throughout the experiment by means of a digital contact thermometer.

3. Survey of the Experiments. (*a*) *Monolayer Stability (referred henceforth as monolayer experiment).* Only the S part of the plate was coated by a LB-DPPA monolayer. Buffer solution was filled into S and R and was kept stationary. In the SBSR mode, DPPA signals were detectable and could be used to monitor the stability of the monolayer in an aqueous environment.

(*b*) *Long-Term Adsorption (referred henceforth as adsorption experiment).* DPPA was deposited onto both S and R. Then a POPC vesicle solution was filled into S and buffer solution into R, thus permitting an in situ detection of the state of POPC adsorption. The vesicle solution in S and the buffer in R were kept stationary, and long-term adsorption of POPC molecules to the DPPA monolayer in S was monitored.

(*c*) *Bilayer Stability (referred henceforth as bilayer experiment).* DPPA was deposited onto S and R. A bilayer was prepared in the S compartment by adsorption of POPC (DPPC). Buffer was filled into R and was kept stationary, whereas a corresponding buffer was pumped through the S cuvettes in a closed cycle. As in the *adsorption* experiment, background-compensated spectra of the second leaflet of the bilayer (POPC or DPPC) were obtained. They were used to investigate the stability of the supported bilayer in a circulating buffer solution.

4. Preparation of Bilayers. Before a new experiment was begun, the ATR plate was polished by hand on a plane support covered with a nylon cloth by means of a diamond paste (0.25 μm). Attention was paid to avoid a preferred polishing direction. Subsequently, the plate was subjected to various cleaning procedures, using (a) triply distilled water and a 4:1 ethanol: chloroform solution alternately, until there were no visible impurities left, and (b) pure ethanol to remove all small particles originating from cellulose toils used in the first cleaning steps. Remaining organic impurities were removed by plasma cleaning (1.5 min, Harrick Sci. Corp.). The germanium ATR plate was considered to be clean if the $\nu(CH_2)$ bands at ~2920 and ~2850 cm^{-1} disappeared completely in the FTIR-ATR spectrum (single beam mode).

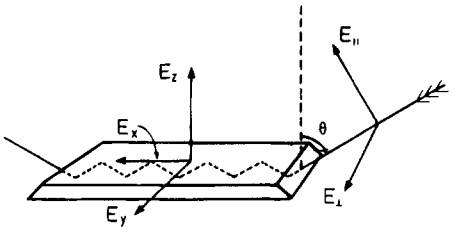

Figure 1. Directions of electric field components of the incident light and the evanescent wave: Θ, angle of incidence; $E_{\parallel}$, $E_{\perp}$, parallel and perpendicular polarized components of the incidence light; E_x, E_y, E_z, electric field components of the evanescent wave in the direction of the coordinate system fixed onto the ATR plate. $E_{\parallel}$ gives rise to E_x and E_z; $E_{\perp}$ gives rise to E_y.[68]

First Leaflet. The first leaflet (DPPA) of the bilayer was transferred via the LB technique onto the ATR plate by a MGW Lauda film balance at 22 ± 2 °C. Surface pressures were measured with an accuracy of 0.1 $mN \cdot m^{-1}$. The ATR plate was fixed to a film lift with the long axis (x-axis, cf. Figure 1) perpendicular to the air−water interface and immersed until the plate area which subsequently was covered by the ATR cuvettes was completely under water. The moving barrier was completely expanded, and a few drops of a DPPA solution (chloroform:methanol = 15:1, ~1 mM, 40 °C) were spread at the air−water interface. After evaporation of the solvent, the DPPA monolayer was slowly compressed to 30 $mN \cdot m^{-1}$. A stability test was performed, keeping the monolayer 10 min at this constant surface pressure in order to monitor an eventual further compression, which in no case was observed.

The compressed film was then deposited onto the ATR plate at a withdrawing speed of 1.8 $mm \cdot min^{-1}$. With this the DPPA molecules attached with their head groups to the hydrophilic surface on both sides of the germanium plate. Withdrawing was stopped when the first edge of the trapezoid's lateral face (the entrance face of the light) reached the air−water interface. Before the lateral face was withdrawn through the air−water interface, the film was expanded as far as possible. This procedure allowed the entrance face to be easily cleaned with chloroform. The ATR plate was mounted in the SBSR cell immediately upon DPPA coating.

The DPPA monolayer on the S part of the ATR plate was then used as substrate for POPC (DPPC) adsorption. But first, SBSR spectra of the DPPA-coated plate were recorded at 25 °C with air-filled cuvettes.

Second Leaflet. About 2 mg of POPC (DPPC) were suspended in 2 mL of buffer. Vesicles were prepared by sonication with an Elgasonic bath sonifier in N_2 atmosphere at ~35 °C (45 °C), i.e. above the corresponding chain melting temperature T_m. After about 20−30 min, the solution was almost completely transparent and was used for preparation of the second leaflet of the bilayer within a maximum of 30 min. Although vesicles had not been characterized with respect to size, shape, or lamellarity, they were expected to be small and unilamellar because of the mode of preparation and their light scattering features.

The clear vesicle solution was filled via a Desaga PLG multiple peristaltic pump at $T > T_m$ into the S compartment of the SBSR cell (POPC, 25 °C; DPPC, 45 °C). At the same time, deaerated buffer was filled into the R compartment. During the filling process the cell was held with the long side of the ATR plate (x-direction; cf. Figure 1) in an upright position, with the solution inlets of the S and R compartments at the bottom. By this, the DPPA monolayer in the S compartment was slowly contacted with the POPC (DPPC) vesicle solution while the surface of the solution moved from the inlets at the bottom to the outlets at the top. The adjusted pumping rate of 170 $\mu L \cdot min^{-1}$ corresponded to a velocity of solution−surface displacement along the immobilized DPPA monolayer of approximately 80 $mm \cdot min^{-1}$. As soon as the vesicle solution in S and the buffer in R reached the outlets of the second cuvettes of the compartments, the pump was turned off, the vesicle and buffer reservoirs were disconnected, and all inlet and outlet tubes were clamped to avoid penetration of air. The cell was now mounted in the spectrometer for 1 h to monitor the short-term POPC (DPPC) adsorption in

the spectrometer by measuring short || polarized spectra (POPC, 25 °C; DPPC, 45 °C).

After that period, which did not seem to be necessary for bilayer preparation (cf. ref 28), a short draining step followed the preparation procedure as a consequence of an optimization based on electron microscopic (EM) information. EM pictures had revealed that fragments of vesicles may remain adsorbed to the resulting bilayer in a nonregular way. These fragments seemed to be rather loosely bound and could be removed by draining the cell shortly after bilayer completion. The remaining membrane looked flat and compact in the EM.[12,16]

For that purpose, the cell was dismounted from the spectrometer and the clamps at the S inlet and outlet were removed. With the cell held in the same upright position with the inlets at the bottom, the vesicle solution in S was displaced by about 2 mL of triply distilled water in order to prevent a formation of small crystals from buffer components during the subsequent draining step. Now the temperature was reduced to 25 °C in the case of DPPC. The cell was turned upside down (outlets at the bottom), and the pump was allowed to suck air. The resulting "air pistons" moving in the S cuvettes downward are believed to remove undesired lipid adsorbates, as has been suggested by EM. As soon as the S compartment was empty, the cell was returned to its original position (inlets at the bottom) and the S compartment was connected to a circulation system containing a vessel with a buffer reservoir of 5–8 mL. No later than about 5 min after the compartment was drained, buffer was filled into the S compartment in the same way as the vesicle solution (t = 0 h). The first few milliliters were flushed through. Thereupon, the outlet tube was connected to the buffer reservoir, resulting in a circulating buffer solution through the S compartment (~170 μL·min^{-1}). The cell was then mounted in the spectrometer, and spectra acquisition was started immediately. Self-built online deaerating equipment was constantly sucking air through a tube through which the circulating buffer was directed, in order to avoid formation of air bubbles in the circulating buffer.

5. Modifications in the Monolayer and Adsorption Experiments. The following changes in the procedure described above should be mentioned. In the *monolayer* experiment, the DPPA film was only deposited onto the S part of the ATR plate. During LB deposition the plate was fixed with the y-axis (cf. Figure 1) perpendicular to the water surface, and only immersed until half-width. After the monolayer compression, the plate was withdrawn from the subphase at a constant surface pressure of 30 mN·m^{-1}. After DPPA deposition, deaerated buffer solution was filled at 25 °C into the S and R compartment (t = 0 h). The tubes were nipped off with clamps, and the cell was placed immediately in the spectrometer to perform the monolayer stability measurement, performed in the stationary aqueous phase.

In the *adsorption* experiment, the DPPA monolayer was deposited in the same way as in the *bilayer* experiment. POPC vesicle solution and buffer were filled at 25 °C into S and R (t = 0 h), respectively, and all inlet and outlet tubes were clamped. The cell was mounted in the spectrometer, and spectra were acquired over a period of about 40 h in order to monitor the long-term adsorption of POPC.

6. Spectra Acquisition and Manipulation. Infrared spectra were recorded with a Bruker IFS 48 FTIR spectrometer equipped with a gold grid polarizer on a KRS-5 substrate and a SBSR-ATR mirror attachment (angle of incidence θ = 45°). The sample compartment of the spectrometer was continuously purged with nitrogen. A deuterium-triglycine-sulfate (DTGS) detector (2 × 2 mm^2) was used. All spectra were scanned at 4 cm^{-1} resolution with a zero filling factor of 4.

After deposition of the LB-DPPA monolayer, SBSR spectra of the DPPA-coated ATR plate were measured. In the *monolayer* experiment, the DPPA spectrum was directly observable in the SBSR mode, whereas in the *adsorption* and *bilayer* experiments no DPPA signals were visible since equal amounts of DPPA had been deposited onto the S and R parts of the ATR plate. However, there was a slight incompensation of DPPA signals detectable in the $\nu(CH_2)$ region, which probably was due to a small inhomogeneity between the S and R beams. Thus, SBSR absorbance spectra of the DPPA-coated ATR plate in the dry state after LB deposition were subtracted from all subsequent SBSR absorbance spectra to correct this slight incompensation (*adsorption* and *bilayer* experiments).

In the *monolayer* experiment, the following manipulation was performed to achieve a spectrum of DPPA in an aqueous environment: the SBSR absorbance spectrum of DPPA in the dry state was scaled by the factor $(N_{DPPA} - N_{aq})/N_{DPPA}$ (N_{DPPA} = 25, total number of internal reflections, N_{aq} = 19.3 number of internal reflections within the cuvette) and subtracted from all SBSR absorbance spectra of DPPA measured after buffer introduction into S and R (|| spectra, 512 scans; ⊥ spectra, 1024 scans). This correction compensated the DPPA LB monolayer outside of the cuvette (O-seal).

In the *adsorption* and *bilayer* experiments, the vesicle solution was filled into S and buffer into R, and SBSR spectra were measured to monitor phospholipid adsorption from the vesicle solution to the DPPA monolayer. In the case of *bilayer* experiments, only the short-term adsorption was observed: || polarized spectra with 128 scans were collected over a period of 1 h, whereas in the *adsorption* experiment, spectra with 512 (||) and 1024 (⊥) scans were acquired alternatingly at 25 °C over a period of 40 h. The SBSR spectra recorded after bilayer preparation at 25 °C for stability tests typically consisted of 1024 (||) or 2048 (⊥) scans (*bilayer* experiments).

SBSR spectra were converted into JCAMP files, transferred to an IBM-compatible PC, and imported into the Spectrafile-Plus 1.1 program from Hayden & Son. The scaling and compensation procedures mentioned above were performed by multiplying and subtracting spectra over the whole range from 4000 to 800 cm^{-1}. The resulting $\nu_s(CH_2)$ bands, which in each case could be assigned to one kind of phospholipid, were integrated without prior smoothing of spectra.

Theoretical Section

Integrated || and ⊥ polarized absorbances of the $\nu_s(CH_2)$ vibration were plotted against time and fitted by adequate analytical expressions (see below). Mean absorbance values were then used to calculate the surface concentration Γ, the molecular area A_{mol}, and the mean molecular order parameter $\bar{S}_{mol}$ as a function of time. Γ [mol·cm^{-2}] was calculated according to eq 1:

$$\Gamma = \frac{a_\perp d}{3\int \epsilon(\tilde{\nu})\, d\tilde{\nu}\, N v d_{e\perp}^{iso}}\left[2 - \frac{E_{0x}^{r2}}{E_{0z}^{r2}} + R\frac{E_{0y}^{r2}}{E_{0z}^{r2}}\right] \quad (1)$$

with

$$d_{e\perp}^{iso} = \frac{n_{21} d_p}{2\cos\theta}(e^{-2z_i/d_p} - e^{-2z_f/d_p})E_{0y}^{r2} \quad (2)$$

and

$$d_p = \frac{1}{2\pi\tilde{\nu} n_1 (\sin^2\Theta - n_{31}^2)^{1/2}} \quad (3)$$

where $d_{e\perp}^{iso}$ = effective thickness of an isotropic sample per internal reflection for perpendicular polarized incident light [cm], d_p = depth of penetration of the evanescent wave [cm], $a_{||,\perp} = \int A_{||,\perp}(\tilde{\nu})\, d\nu$ = integrated absorbance for ⊥ and || polarized incident light, respectively [cm^{-1}], $A_{||,\perp}$ = absorbance for || and ⊥ polarized incident light, respectively, $\tilde{\nu} = 1/\lambda$ = wavenumber of the IR beam in vacuum [$\nu_s(CH_2)$]: $\tilde{\nu}$ = [2850 cm^{-1}], λ = wavelength of IR beam in vacuum [cm], $R = a_{||}/a_\perp$ = dichroic ratio, $d = z_f - z_i$ = thickness of the layer (monolayer), ranging from z_i to z_f, z_i, z_f = initial (i) and final (f) z-coordinates of the

(16) Kopp, F.; Fringeli, M.; Goette, J.; Fringeli, U. P. In preparation.

(17) For a detailed discussion of the calculation of the surface concentration Γ and the mean molecular order parameter $\bar{S}_{mol}$ as well as for error analysis, see the Appendix.

layer [DPPA, $z_i = 0$ cm; $z_f = 2.5 \times 10^{-7}$ cm; DPPC, POPC, $z_i = 2.5 \times 10^{-7}$ cm; $z_f = 5.0 \times 10^{-7}$ cm], $\int \epsilon(\tilde{\nu})\, d\tilde{\nu}$ = integrated molar absorption coefficient. For $\nu_s(CH_2)$ per methylene group at 25 °C $\int \epsilon(\tilde{\nu})\, d\tilde{\nu} = 5.92 \times 10^5$ cm·mol^{-1} (ref 18), N = mean number of internal reflections within the cuvette (active internal reflections) [in this case, phospholipids that are in contact with the buffer solution: $N = 19.3$], ν = number of functional groups (methylene groups) per molecule [DPPA, 30; DPPC, POPC, 32], $n_{ik} = n_i/n_k$ = ratio of refractive indices of media i and k [Ge-ATR-plate) $n_1 = 4.00$; phospholipid membrane, $n_2 = 1.45$; buffer solution, n_3 (2850 cm^{-1}) = 1.41, anomalous dispersion[12], θ = angle of incidence [45°], E^r_{0x}, E^r_{0y}, E^r_{0z} = relative electric field components at $z = 0$ cm (for calculation see "thin film approximation" in ref 12).

The molecular area of a phospholipid, A_{mol} was calculated from its respective surface concentration by

$$A_{mol} = \frac{10^{16}}{\Gamma(6.022 \times 10^{23})} \quad (4)$$

(dim Γ = mol·cm^{-2}, dim A_{mol} = Å^2·molecule^{-1}).

The mean molecular order parameter $\bar{S}_{mol}$ was calculated according to

$$\bar{S}_{mol} = \frac{4(E^{r2}_{0x} - RE^{r2}_{0y} + E^{r2}_{0z})}{(3\cos^2\Theta - 1)(3\cos^2\delta - 1)(E^{r2}_{0x} - RE^{r2}_{0y} - 2E^{r2}_{0z})} \quad (5)$$

and symbols not yet defined are Θ = angle between the transition dipole moment of a given vibration (e.g. $\nu_s(CH_2)$) and the molecular axis (e.g. hydrocarbon chain segment, $\Theta = 90°$), δ = angle between the bilayer normal and the average orientation of the molecular axis (e.g. hydrocarbon chains in the gel state (tilt angle)).

The determination of $\bar{S}_{mol}$ of POPC in the liquid crystalline phase as well as of DPPA in the gel phase (no chain tilt expected) was performed by means of eq 5 under the assumption of $\delta = 0°$. In the case of DPPC in the gel phase, only a set of mutually dependent $\bar{S}_{mol}/\delta$ value pairs should be determined. Equation 5 was then used to calculate the tilt angle δ since $\bar{S}_{mol}$ could be assessed through $\bar{S}_{mol}$ of DPPA because the latter was also in the gel phase and did not exhibit a chain tilt.

Results and Discussion

Supported bilayers have been prepared in two steps as outlined in the Experimental Section. Properties of the first leaflet before bilayer completion as well as properties of the second leaflet after bilayer completion were evaluated spectroscopically in subsequent experiments.

DPPA Monolayer. The first leaflet (DPPA) of the supported bilayer was prepared via LB monolayer deposition onto the ATR plate in the LB trough. Figure 2a presents || and ⊥ polarized SBSR spectra of the DPPA monolayer in an air environment, measured after the deposition (Cf. *monolayer* experiment in the Experimental

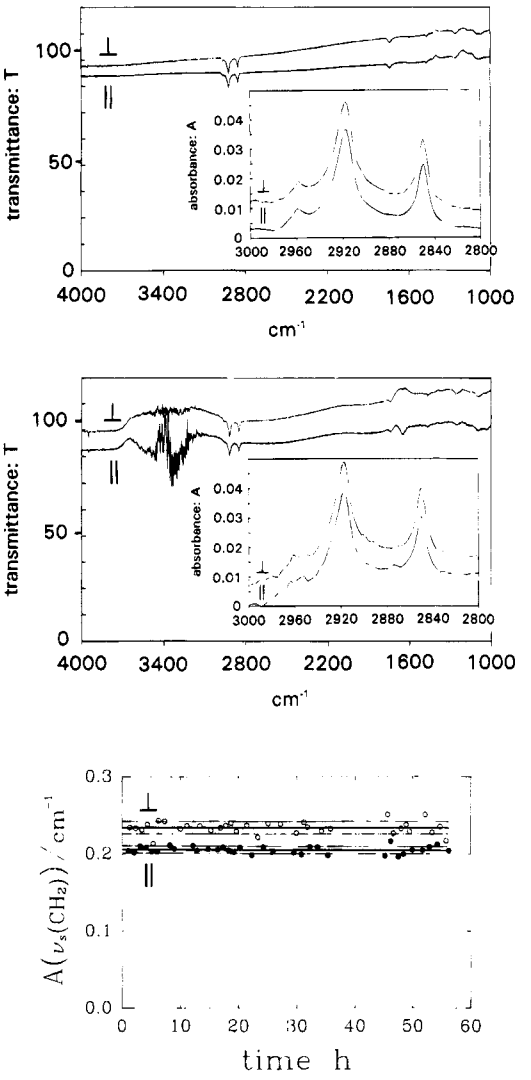

Figure 2. (a, Top) || and ⊥ polarized SBSR transmittance spectra of the LB-DPPA monolayer on the germanium ATR plate in an air environment (cf. *monolayer* experiment in the Experimental Section). S: LB-DPPA monolayer in an air environment. R: blank ATR plate in an air environment. Insert: || and ⊥ polarized SBSR absorbance spectra of the ν(CH) region. Angle of incidence $\Theta = 45°$; mean number of DPPA-sensing internal reflections, $N_{DPPA} = 25°$; $T = 25$ °C; resolution = 4 cm^{-1}; number of scans = (||) 5632 and (⊥) 3584. (b, Middle) || and ⊥ polarized SBSR transmittance spectra of the same DPPA monolayer as in part a in buffer solution, ~55 h after buffer introduction (cf. *monolayer* experiment in the Experimental Section). S: LB-DPPA monolayer in stationary buffer. R: blank ATR plate in stationary buffer. Insert: || and ⊥ polarized SBSR absorbance spectra of the ν(CH) region. Absorbance spectra of part a had been scaled with $(N_{DPPA} - N_{aq})/N_{DPPA}$ and subtracted from the SBSR absorbance spectra in buffer environment in order to compensate for the contribution of DPPA in an air environment outside the area covered by the S and R cuvettes. Angle of incidence $\theta = 45°$; mean number of DPPA in buffer environment-sensing internal reflections, $N_{aq} = 19.3$; mean number of DPPA-sensing internal reflections, $N_{DPPA} = 25$; buffer = 20 mN Na_2HPO_4/NaH_2PO_4 pH = 7.0, 100 mM NaCl, 0.1 mM $CaCl_2$; $T = 25$ °C; resolution = 4 cm^{-1}; number of scans = (||) 512 and (⊥) 1024. (c, Bottom) Time course of || and ⊥ polarized integrated absorbances of the $\nu_s(CH_2)$ vibration measured in SBSR absorbance spectra of the DPPA monolayer on germanium in buffer solution (cf. part b). Functions used to fit the data points (t in hours): $\hat{A}_{||}(t) = 0.206 - (2.45 \times 10^{-5})t$ and $\hat{A}_{\perp}(t) = 0.234 - (1.02 \times 10^{-5})t$. Thin lines below and above the fit functions denote the standard deviations: $\hat{A}_{||}(t) \pm s(\hat{A}_{||}(t))$ and $\hat{A}_{\perp}(t) \pm s(\hat{A}_{\perp}(t))$, respectively (cf. eq 22).

(18) The integrated molar absorption coefficient $\int \epsilon^*(\tilde{\nu})\, d\tilde{\nu}$ of the $\nu_s(CH_2)$ mode had been determined to be 6.51×10^5 cm·mol^{-1} for fatty acids at 25 °C. Since the $\nu_s(CH_2)$ and the week $\nu_s(CH_3)$ band overlapped slightly, integration of the $\nu_s(CH_2)$ band was performed with a fixed left integration limit of 2867.0 cm^{-1} (DPPA, DPPC) or 2869.9 cm^{-1} (POPC) in order to avoid a contribution of the $\nu_s(CH_3)$ vibration to the dichroic ratio of $\nu_s(CH_2)$ and the calculation of $\bar{S}_{mol}$. This "restricted integration" required a corresponding adaptation of the integrated absorption coefficient. Through a comparison of integrated absorbances obtained by full and restricted integration of $\nu_s(CH_2)$ of DPPA, the relation between the two coefficients was found to be about 1.1 $\int \epsilon(\tilde{\nu})\, d\tilde{\nu} = \int \epsilon^*(\tilde{\nu})\, d\tilde{\nu}$. For a more accurate interpretation of the spectra, the above-mentioned overlapping bands should be fitted with two components prior to integration, a procedure which was not applied because of the great amount of spectra.

Table 1. Properties of the Prepared Monolayer/Bilayers at 25 °C

	surface conc $\Gamma \pm$ st dev[c] (mol·cm^{-2})		mol area $A_{mol} \pm$ st dev[c] (Å^2·molecule^{-1})		mean mol order param $\bar{S}_{mol}$ ($\delta = 0°$) $\pm$ st dev[c]		
	$t = 0$ h	$t \sim 60$ h	$t = 0$ h	$t \sim 60$ h	$t = 0$ h	$t \sim 60$ h	tilt angle δ[d]
1st leaflet[a]							
DPPA	$3.97 \times 10^{-10} \pm 0.06$	$3.95 \times 10^{-10} \pm 0.06$	41.8 ± 0.6	42.0 ± 0.6	0.97 ± 0.05	0.97 ± 0.05	~0°
2nd leaflet[b]							
POPC (25 °C)	$2.20 \times 10^{-10} \pm 0.04$	$2.20 \times 10^{-10} \pm 0.04$	75.5 ± 1.4	75.5 ± 1.4	0.30 ± 0.07	0.25 ± 0.07	
DPPC (45 °C)	$4.55 \pm 10^{-10} \pm 0.05$	$3.94 \pm 10^{-10} \pm 0.05$	36.5 ± 0.4	42.1 ± 0.5	0.72 ± 0.04	0.73 ± 0.04	≤24°

[a] Monolayer in buffer environment. [b] Leaflet prepared by adsorption from vesicle solution; values in parentheses denote the temperature during the adsorption period. [c] Standard deviations were computed according to eqs 23, 24, 25ab, 26ab, and 27 in the Appendix. [d] A tilt was only assumed for DPPC and was calculated by means of eq 5. DPPA could not be tilted substantially because of its high $\bar{S}_{mol}$ value.

Section). The spectral range from 3000 to 2800 cm^{-1} is depicted in the insert. Bands at 2959, 2917, and 2850 cm^{-1} are assigned to $\nu_{as}(CH_3)$, $\nu_{as}(CH_2)$, and $\nu_s(CH_2)$ modes, respectively. A $\nu_s(CH_3)$ band (at about 2873 cm^{-1}) is not visible.[19]

Spectra of the same DPPA monolayer in contact with buffer solution are depicted in Figure 2b. Incompensation of the water bands at ~3400 cm^{-1} (ν(OH)) and ~1640 cm^{-1} (δ(OH)) is predominantly due to the fact that water molecules are partially excluded from the evanescent wave in the S part because of the DPPA monolayer, as well as to the different physical states of water molecules in contact with the hydrophobic acyl chains of DPPA in the S part and the hydrophilic germanium in the R part of the ATR plate.

Like in an air environment (Figure 2a), a high degree of hydrocarbon chain ordering is apparent from ATR dichroism of the $\nu_{as}(CH_2)$ and the $\nu_s(CH_2)$ bands in a buffer environment (Figure 2b). The stability of the DPPA monolayer in a stationary buffer solution was monitored over a period of about 60 h by acquiring alternatively $\parallel$ and $\perp$ polarized SBSR spectra. Integrated absorbances of the $\nu_s(CH_2)$ band were fitted by straight lines (cf. Figure 2c). Applying the formulas given in the theoretical section allowed the time courses of the surface concentration Γ, the molecular area A_{mol}, and the mean molecular order parameter $\bar{S}_{mol}$ ($\delta = 0°$) to be calculated from the fitted integrated absorbances, and these are listed in Table 1. It was found that the surface concentration remained almost constant during the period of observation. This finding is in contrast with a partial detaching of DPPA molecules in a circulating buffer solution (data not shown). The determined surface concentration of $\Gamma = 3.97 \times 10^{-10}$ mol·cm^{-2} corresponds to a molecular area $A_{mol} = 41.8$ Å^2, which is in good agreement with the value given by Demel et al., who determined an area of 43.8 Å^2·molecule^{-1} for a DPPA monolayer at the air–water interface at pH = 7.2 and a surface pressure above 30 mN·m^{-1}.[20] It should be noted that, in contrast to $\bar{S}_{mol}$, the surface concentration Γ can be determined with rather high accuracy, as is evident from the standard error intervals given in the table.

DPPA was in the gel phase ($T_m \sim 65$ °C).[53] Nevertheless, the liquid crystalline phase model (eq 5; $\delta = 0°$) was applied to calculate $\bar{S}_{mol}$ since no chain tilt was expected for DPPA in the gel state because the area occupied by the head group is not larger than the sum of the cross sections of the two hydrocarbon chains.[21] A remarkably high degree of order was observed: $\bar{S}_{mol}$ assumed a value of 0.97 anddid not change significantly over the period of measurement. It is concluded that hydrocarbon chains of DPPA indeed could not be tilted and were essentially in the all-trans state.

Finally, it should be noted that atomic force microscopy (AFM) studies in the same buffer have confirmed a stable monolayer structure of DPPA on glass, a substrate with surface properties similar to those of germanium. On mica, however, island formation was found by AFM, most probably because of the negative charge of this substrate (data not shown).

DPPA/POPC Bilayer. For the preparation of the second leaflet of a supported DPPA/POPC bilayer, a POPC vesicle solution was contacted slowly and in a controlled manner with the LB-DPPA monolayer on the ATR plate. Thereby, POPC molecules spontaneously self-organized and built up the second leaflet of the bilayer.

(1) Long-Term POPC Adsorption. The long-time adsorption of POPC from the vesicle solution to the DPPA monolayer was monitored after the S compartment was filled with the vesicle solution (cf. *adsorption* experiment in the Experimental Section). Figure 3a shows $\parallel$ and $\perp$ polarized SBSR spectra of POPC adsorbed to the DPPA monolayer. The insert displays the ν(CH) region of $\parallel$ polarized spectra at successive stages of adsorption. In addition to the adsorbed POPC, bulk POPC vesicles also contributed slightly to the overall POPC absorbance. The $\parallel$ and $\perp$ integrated absorbances of a 1 mg·mL^{-1} POPC vesicle solution under the given experimental conditions were calculated to be 0.011 and 0.006 cm^{-1}, respectively. These values were subtracted from the overall integrated absorbances of the $\nu_s(CH_2)$ band in order to obtain unperturbed integrated absorbances of the adsorbed POPC. The latter are plotted in Figure 3b as a function of time.

Apparently, the adsorption of POPC molecules to the hydrocarbon chains of the immobilized DPPA monolayer exhibited two different kinetic phases. In a first, very rapid step, adsorption proceeded up to a surface concentration of about 2.5×10^{-10} mol·cm^{-2} (extrapolation: $t \rightarrow 0$; cf. Figure 3c), which is equivalent to a molecular area A_{mol} for POPC of 66 Å^2. The mean molecular area of egg lecithin, which contains about 70% POPC,[22] has been determined to be 68–75 Å^2.[23] Thus, the above finding suggests the rapid adsorption of POPC stopped when a POPC monolayer had formed on the hydrophobic surface of the LB-DPPA, which prevented the DPPA hydrocarbon chains from water contact.

In a second phase, a slow and partial multilayer adsorption is visible. Equilibrium was not attained within 30 h. At this stage, the surface concentration (4.0×10^{-10} mol·cm^{-2}; cf. Figure 3c) amounted to 1.6–1.8 adsorbed POPC monolayers, it is believed that, instead of an association of DPPA and POPC hydrocarbon chains during

(19) Mendelsohn, R.; Mantsch, H. H. In *Progress in Protein–Lipid Interactions Vol. 2*; Watts, A., de Pont, J. J. H. H. M., Eds.; Elsevier: Amsterdam, 1986; p 103.
(20) Demel, R. A.; Yin, C. C.; Lin, B. Z.; Hauser, H. *Chem. Phys. Lipids* **1992**, *60*, 209.
(21) Hauser, H.; Pascher, I.; Pearson, R. H.; Sundell, S. *Biochim. Biophys. Acta* **1981**, *650*, 21.
(22) Tattrie, N. H.; Bennett, J. R.; Cyr, R. *Can. J. Biochem.* **1968**, *46*, 819.
(23) Rand, R. P. *Annu. Rev. Biophys. Bioeng.* **1981**, *10*, 277.

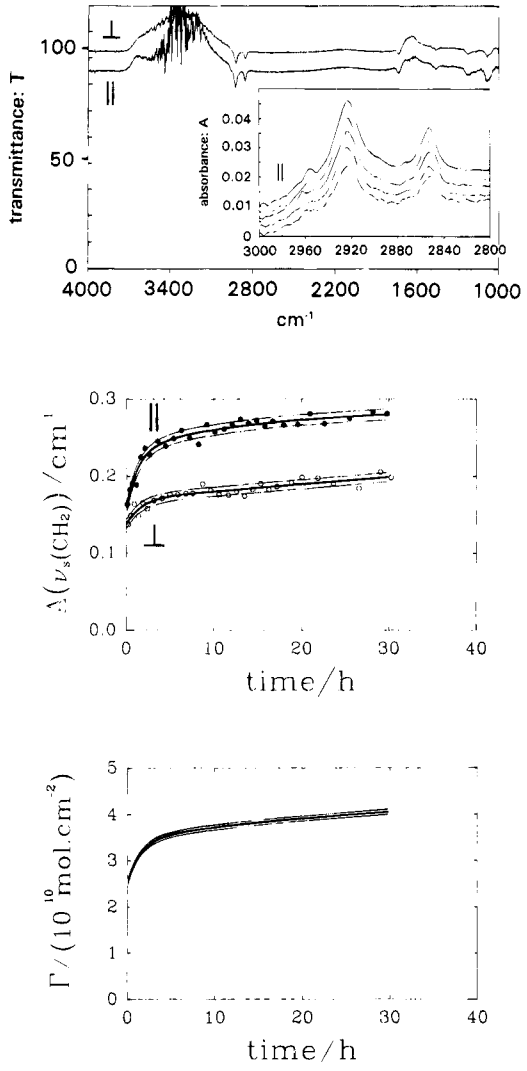

Figure 3. (a, Top) || and ⊥ polarized SBSR transmittance spectra of POPC adsorbed to a DPPA monolayer, measured after a 31 h adsorption period in POPC vesicle solution (~1 mg·mL^{-1}; cf. *adsorption* experiment in the Experimental Section). The spectra contain a small contribution due to the bulk vesicle solution. S: LB-DPPA monolayer on germanium, adsorbed POPC, stationary POPC vesicle solution. R: LB-DPPA monolayer on germanium, stationary buffer solution. Insert: || polarized SBSR absorbance spectra of the ν(CH) region at successive stages of adsorption (from bottom to top: $t = 0.4$, 1.0, 3.0, 11.5, 31.1 h). Angle of incidence $\theta = 45°$; mean number of POPC-sensing internal reflections, $N_{aq} = 19.3$; vesicle solution = 20 mM Na_2HPO_4/NaH_2PO_4 pH = 7.0, 100 mM NaCl, 0.1 mM $CaCl_2$; $T = 25$ °C; resolution = 4 cm^{-1}; number of scans = (||) 512 and (⊥) 1024. (b, Middle) Time course of the contributions of adsorbed POPC to the || and ⊥ polarized integrated absorbances of the $\nu_s(CH_2)$ band, observed in SBSR spectra of POPC adsorbed to the DPPA monolayer in vesicle solution (cf. part a). Functions used to fit the data points (t in hours): $\hat{A}_{||}(t) = 0.158 + 0.052(1 - e^{-0.068t}) + 0.076(1 - e^{-0.730t})$ and $\hat{A}_{\perp}(t) = 0.137 + 0.210(1 - e^{-0.0049t}) + 0.033(1 - e^{-0.600t})$. Thin lines below and above the fit functions denote the standard deviations $\hat{A}_{||}(t) \pm s(\hat{A}_{||}(t))$ and $\hat{A}_{\perp}(t) \pm s(\hat{A}_{\perp}(t))$ (cf. eq 22). (c, Bottom) Increase of the surface concentration $\hat{\Gamma}(t)$ of POPC adsorbing from the vesicle solution to the DPPA monolayer, calculated from $\hat{A}_{||}(t)$ and $\hat{A}_{\perp}(t)$ (cf. part b) by means of eq 1. Thin lines below and above $\hat{\Gamma}(t)$ denote the standard deviation $\hat{\Gamma}(t) \pm s(\hat{\Gamma}(t))$, assessed by means of eqs 24 and 26a,b.

the first phase, a head-group-to-head-group association between POPC and molecules accounted for this partial multilayer adsorption.

Phospholipid bilayers experience a strongly repulsive, exponentially decaying "hydration force", consequent to

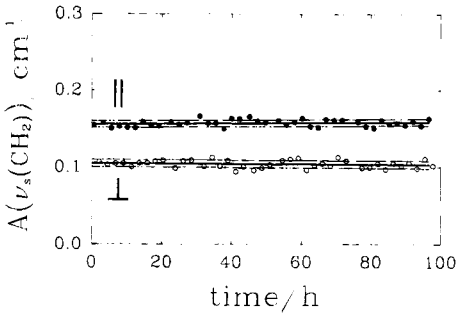

Figure 4. Time course of the || and ⊥ polarized integrated absorbances of the $\nu_s(CH_2)$ band, observed in SBSR spectra of POPC, adsorbed to DPPA, measured after the bilayer preparation procedure in buffer solution. R: LB-DPPA monolayer on germanium, stationary buffer solution. Functions used to fit the data points (t in hours): $\hat{A}_{||}(t) = 0.156 + (2.62 \times 10^{-5})t$ and $\hat{A}_{\perp}(t) = 0.105 - (2.31 \times 10^{-5})t$. Thin lines below and above the fit functions denote the standard deviations $\hat{A}_{||}(t) \pm s(\hat{A}_{||}(t))$ and $\hat{A}_{\perp}(t) \pm s(\hat{A}_{\perp}(t))$ (cf. eq 22). Angle of incidence $\theta = 45°$; mean number of POPC-sensing internal reflections, $N_{aq} = 19.3$; buffer = 20 mM Na_2HPO_4/NaH_2PO_4 pH = 7.0, 100 mM NaCl, 0.1 mM $CaCl_2$; $T = 25$ °C; resolution = 4 cm^{-1}; number of scans = (||) 1024 and (⊥) 2048.

the work of removing water from the polar head groups.[24] Below a mutual distance of 20–30 Å, this force dominates any electrostatic repulsion between two membranes[25] and poses a significant energetic barrier to bilayer contact.[26] This "hydration force" could have been the reason for the observed slowness of multilayer adsorption.

When the POPC vesicle solution was left at room temperature for 1–2 days, it became turbid, and vesicle sedimentation was visible. It is known that small egg phosphatidylcholine vesicles formed upon sonication are unstable and fuse over time to large multilamellar structures with less narrow curvature,[27] probably because the space requirements for the head group and the acyl chains are about the same in the liquid crystalline phase.[21] Consequently, sedimentation of POPC vesicles in the ATR cell might have diminished the vesicle concentration in the S compartment, thereby slowing down the long-term adsorption.

(*2*) *Preparation of a DPPA/POPC Bilayer.* In order to prepare an asymmetric supported DPPA/POPC bilayer, POPC adsorption was stopped after 1 h, vesicle solution was displaced by pure water, the cuvettes were flushed with air, and buffer was filled in again (cf. *bilayer* experiments in the Experimental Section).[28] The stability of the resulting DPPA/POPC bilayer in a circulating buffer solution was monitored by measuring spectra of the POPC leaflet which was in contact with the buffer solution. Figure 4 displays the time course of the || and ⊥ integrated absorbances of $\nu_s(CH_2)$; Γ, A_{mol}, and $\bar{S}_{mol}$ were computed as stated above.

The DPPA/POPC bilayer was monitored over a period of 100 h. It turned out to be remarkably stable in a

(24) Lis, L. J.; McAlister, M.; Fuller, N.; Rand, R. P.; Parsegian, V. A. *Biophys. J.* **1982**, *37*, 657.
(25) Cowley, A. C.; Fuller, N.; Rand, R. P.; Parsegian, V. A. *Biochemistry* **1978**, *17*, 3163.
(26) LeNeveu, D. M.; Rand, R. P.; Parsegian, V. A. *Nature* **1976**, *259*, 601.
(27) Tenchov, B. G.; Yanev, T. K.; Tihova, M. G.; Koynova, R. D. *Biochim. Biophys. Acta* **1985**, *816*, 122.
(28) Because of the limited sensitivity of the DTGS detector, only || polarized spectra were acquired during the adsorption phase. Thus, no surface concentration could be determined. However, the integrated absorbance at the end of the adsorption time was equal to $\hat{A}_{||}(t)$ at $t =$ 0 h after the bilayer preparation procedure (~0.15 cm^{-1}), indicating similar surface concentrations before and after the draining step. The integrated absorbance at the beginning of the adsorption period was only slightly lower.

circulating buffer solution. For the POPC leaflet, a constant surface concentration of 2.20×10^{-10} mol·cm^{-2} was determined. This is equivalent to a molecular area $A_{mol} = 75.5$ Å^2, compared to ~66 Å^2·molecule^{-1} obtained by extrapolation of Γ to $t = 0$ h in the long-term adsorption experiment (see above). The value of 75 Å^2·molecule^{-1} lies at the upper limit of the range reported for the mean A_{mol} value of egg lecithin.[23] It is concluded that the LB-DPPA monolayer was covered with a POPC monolayer, resulting in an asymmetric DPPA/POPC bilayer.

The mean molecular order parameter $\bar{S}_{mol}$ ($\delta = 0°$) was 0.30 at $t = 0$ h (cf. Table 1). This is considerably lower than $\bar{S}_{mol}$ determined for the DPPA monolayer, $\bar{S}_{mol} = (0.97)$,[29] obviously because POPC was in the liquid crystalline phase ($T_m = -5$ °C). Akutsu et al. and Holmgren et al. reported $\bar{S}_{CH_2}$ values of −0.11 and −0.15 for 1,2-dioleoyl-*sn*-glycero-3-phosphatidylcholine (DOPC).[30,31] These $\bar{S}_{CH_2}$ values correspond to $\bar{S}_{mol}$ values of 0.22 and 0.30 (cf. eq 11; $\Theta = 90°$, Figure 6b). Because of the additional cis double bond in DOPC, a slightly higher mean molecular order parameter was expected for POPC than for DOPC, which seems to be the case indeed. Apparently, the interaction of the two opposing leaflets was negligible in this case; that is, no substantial ordering effect of DPPA on POPC is visible. During the period of measurement, $\bar{S}_{mol}$ decreased slightly, perhaps because the POPC leaflet accumulated small amounts of organic impurities from the circulating buffer solution.

DPPA/DPPC Bilayer. An asymmetric DPPA/DPPC bilayer, with both leaflets in the gel state, was prepared in the same way as the DPPA/POPC bilayer (cf. *bilayer* experiments in the Experimental Section). However, a temperature of 45 °C was chosen during the adsorption of DPPC to the LB-DPPA monolayer in order to perform vesicle adsorption above the main transition temperature of DPPC (41.5–42 °C),[32,33] as it has been done in the case of POPC. After the adsorption period, the SBSR cell was cooled to 25 °C to carry out the stability measurements in circulating buffer solution as in previous experiments. Figure 5a presents spectra of the DPPC leaflet, and Figure 5b displays the time dependence of the integrated absorbances of the DPPC leaflet during buffer circulation, while the calculated Γ and $\bar{S}_{mol}$ ($\delta = 0°$) values are given in Table 1.

In contrast to the DPPA/POPC bilayer, a small amount of initially adsorbed DPPC desorbed from the DPPA/DPPC membrane during the period of observation (cf. Figure 5b). The surface concentration decreased from 4.55×10^{-10} mol·cm^2 at $t = 0$ h to 3.94×10^{-10} mol/cm^2 at $t = 60$ h (corresponding molecular areas: 36.5 and 42.1 Å^2). Desorption equilibrium was almost attained at $t = 60$ h since extrapolation of $t \to \infty$ does not change Γ significantly. Apparently, a partial multilayer adsorption had occurred during the adsorption period, since 36 Å^2 is smaller than the cross section of a DPPC molecule. Partial fragment adsorption and/or an increased adsorption rate of DPPC to the completed DPPA/DPPC bilayer at 45 °C compared to POPC seems to have accounted for the greater extent of adsorption.

A $\bar{S}_{mol}$ value of 0.72–0.73 was determined under the (ad hoc) assumption $\delta = 0°$. This is significantly lower than $\bar{S}_{mol}$ of DPPA and compares favorably with order parameters given in the literature: for DPPC multilayers below T_m, Hübner and Mantsch obtained a value of 0.7, whereas Okamura et al. measured 0.78 and 0.71 for the same type of sample.[34–36]

IR spectra feature the time-resolved (time scale: 10^{-13}–10^{-14} s) distribution of chain orientations. They can be interpreted on the basis of stiff and permanently tilted chains ($\bar{S}_{mol} = 1$; $\delta > 0$) or dynamic angular fluctuations of nontilted chains ($\bar{S}_{mol} < 1$; $\delta = 0$), including all transitions in between (cf. eq 13). FTIR studies on the thermotropic behavior of specifically deuterated DPPC multibilayers in the hydrated state indicate that acyl chains are extended and contain no substantial population of gauche conform-

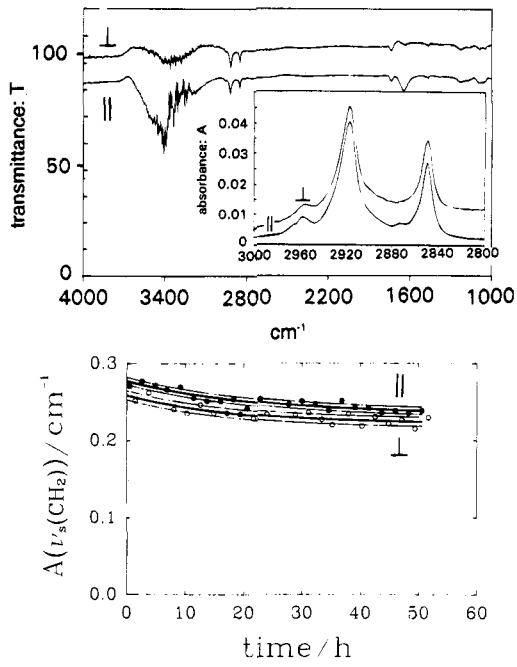

Figure 5. (a, Top) ∥ and ⊥ polarized SBSR transmittance spectra of DPPC adsorbed at 45 °C to the DPPA monolayer, measured in circulating buffer solution ~51 h after bilayer preparation (cf. *bilayer* experiment in the Experimental Section). S: LB-DPPA monolayer on germanium, adsorbed DPPC, circulating buffer solution. R: LB-DPPA monolayer on germanium, stationary buffer solution. Insert: ∥ and ⊥ polarized SBSR absorbance spectra of the ν(CH) region. Angle of incidence $\theta = 45°$; mean number of DPPC-sensing internal reflections, $N_{aq} = 19.3$; buffer = 20 mM Na_2HPO_4/NaH_2PO_4 pH = 7.0, 100 mM NaCl, 0.1 mM $CaCl_2$; $T = 25$ °C; resolution = 4 cm^{-1}; number of scans = (∥) 2048 and (⊥) 2048. (b, Bottom) Time course of the ∥ and ⊥ polarized integrated absorbances of the $\nu_s(CH_2)$ band, observed in SBSR spectra of DPPC adsorbed at 45 °C to the DPPA monolayer, measured in circulating buffer solution after bilayer preparation (cf. *bilayer* experiments in the Experimental Section). S: LB-DPPA monolayer on germanium, adsorbed DPPC, circulating buffer solution. R: LB-DPPA monolayer on germanium in stationary buffer solution. Functions used to fit the data points (t in hours): $\hat{A}_{\parallel}(t) = 0.277 - 0.043(1 - e^{-0.045t})$ and $\hat{A}_{\perp}(t) = 0.259 - 0.036(1 - e^{-0.056t})$. Thin lines below and above the fit functions denote the standard deviations $\hat{A}_{\parallel}(t) \pm s(\hat{A}_{\parallel}(t))$ and $\hat{A}_{\perp}(t) \pm s(\hat{A}_{\perp}(t))$. Angle of incidence $\theta = 45°$; mean number of DPPC-sensing internal reflections, $N_{aq} = 19.3$; buffer = 20 mM Na_2HPO_4/NaH_2PO_4 pH = 7.0, 100 mM NaCl, 0.1 mM $CaCl_2$; $T = 25$ °C; resolution = 4 cm^{-1}; number of scans = (∥) 2048 and (⊥) 2048.

(29) It should be noted because of the enhancement of the variation of $\bar{S}_{mol}$ for almost nonoriented samples (eq 26ab), $\bar{S}_{mol}$ values of POPC are less accurate than $\bar{S}_{mol}$ values of DPPA.

(30) Akatsu, H.; Kyogoku, Y.; Nakahara, H.; Fukuda, K. *Chem. Phys. LIpids* **1975**, *15*, 222.
(31) Holmgren, A.; Johansson, L. B. Å.; Lindblom, G. *J. Phys. Chem.* **1987**, *91*, 5298.
(32) Blume, A. *Biochemistry* **1983**, *22*, 5436.
(33) Chapman, D.; Williams, R. M.; Ladbrooke, B. D. *Chem. Phys. Lipids* **1967**, *1*, 445.
(34) Hübner, W.; Mantsch, H. H. *Biophys. J.* **1991**, *59*, 1261.
(35) Okamura, E.; Umemura, J.; Takenaka, T. *Biochim. Biophys. Acta* **1990**, *1025*, 94.
(36) Okamura, E.; Umemura, J.; Takenaka, T. *Vibrational Spectrosc.* **1991**, *2*, 95.

ers in the gel state.[37] By means of Raman spectroscopy, 1−1.3 gauche conformers per chain have been estimated for DPPC between 30 and 40 °C.[38] As our FTIR-ATR measurements were performed at 25 °C, an even lower mean fraction of gauche conformers was expected. In addition to that, gauche conformers probably occur vastly at the C(14)−C(15) bond and thus do not fully contribute to $\bar{S}_{mol}$. For these reasons, the lower $\bar{S}_{mol}$ value of DPPC compared to DPPA is reasonably assigned to a tilted nearly all-trans chain conformation of DPPC. This is also in good accordance with studies that predict tilted DPPC hydrocarbon chains in the gel phase.[21,53]

Hydrocarbon chains of DPPA were not tilted. It follows that the extent of angular fluctuations could be directly quantified by $\bar{S}_{mol} = 0.97$. In order to assess the tilt angle δ of the DPPC chains, it was assumed that at 25 °C the amplitudes of the dynamic fluctuations of DPPC chain segments (T_m = 42 °C) were at least as great as for DPPA (T_m = 65 °C); that is, $\bar{S}_{mol}$(DPPC; $\delta \neq 0°$) ≤ $\bar{S}_{mol}$(DPPA; $\delta = 0°$) = 0.97. Inserting the dichroic ratio R of the $\nu_s(CH_2)$ band determined in DPPC spectra together with $\bar{S}_{mol} \leq 0.97$ into eq 5 leads to a tilt angle $\delta \leq 24°$.[39]

Since the area occupied by the head group of phosphatidylcholines in the gel phase (~50 Å^2) is larger than the sum of the cross sectional areas of the two hydrocarbon chains (~40 Å^2), packing requires the mutual accommodation of head group lattice and chain matrix. This can be achieved by a space-saving arrangement of head groups (e.g. saw-toothlike). Alternatively, chains must tilt to accommodate the more spacious, layer-aligned head group lattice, thereby establishing an appropriate close-packing contact in the chain matrix.[21] The molecular area A_{mol}, the cross sectional area of a hydrocarbon chain perpendicular to the chain A_{chain}, and the tilt angle δ are related by the equation[21]

$$A_{mol} \cos \delta = 2A_{chain} \quad (6)$$

Consequently, a molecular area of about 41−46 Å^2 had to be expected for a tilt angle of 24° (A_{chain} = 18.5−21 Å^2·chain^{-1}).[21] This value agrees well with A_{mol} = 42.1 Å^2·molecule^{-1}, determined at t = 60 h, near the desorption equilibrium (see above).

During adsorption from the vesicle solution at 45 °C, DPPC was in the liquid crystalline phase, thus exhibiting a molecular area of about 60−70 Å^2.[21] As the membrane was cooled to 25 °C immediately afterwards, DPPC passed through the main transition which is associated with a reduction of the cross sectional area of its hydrocarbon chains. This probably gave rise to a lateral tension (A_{mol} tended to decrease), and the lateral pressure became smaller than its two-dimensional equilibrium pressure,[7] which in principle could be compensated by a corresponding hydrocarbon chain tilt. The rather small size of the observed chain tilt, however, suggests that reduction of the area of the DPPC layer was not exclusively compensated by a hydrocarbon chain tilt (in this case δ = 46° would have been expected at least) but indicates that additionally adsorbed DPPC molecules penetrated into the DPPC leaflet upon passing through the main transition. Table 1 summarizes the results of performed experiments.

Possible Mechanisms of Bilayer Formation. In principle, there should be two different methods of formation of the second leaflet of the supported bilayer, namely, direct adsorption of lipid molecules to the immobilized DPPA monolayer, e.g. via vesicle disruption and adsorption of monomers/multimers, or adsorption of lipid molecules to the surface of the vesicle solution and subsequent "LB-like" deposition of a compact surface monolayer onto the immobilized DPPA monolayer upon movement of the solution's surface along the ATR plate during cell filling.

It is known that phospholipid molecules can adsorb to the surface of aqueous lipid dispersions as well as the surface of vesicle solutions. Depending on the temperature, formation of a surface monolayer, bilayer, or multilayer has been reported.[40−42] Below T_m, adsorption of lipid molecules to the surface of a lipid dispersion[41,43,44] or a vesicle solution[45] is ineffective. Between T_m and T_c, a critical temperature that is characteristic of the phospholipid, the surface concentration increases continuously up to a value at T_c which corresponds to a surface bilayer. On a long time scale, a surface-catalyzed multilayer formation at the air−water interface of a DMPC vesicle solution has been reported at T_c.[42] Further increasing the temperature leads to a decrease of the surface concentration until a value which corresponds to a condensed monolayer.[44]

In the DPPA/DPPC bilayer preparation experiment, DPPC was adsorbed to the DPPA monolayer above T_m at 45 °C, which is almost the critical temperature of DPPC ($T_c \cong$ 44 °C[44]). However, formation of a surface bilayer or even a multilayer seems unlikely because the time scale of the formation of such structures[42,44] is long compared to the handling procedure in our experiments. Besides, the surface area of the vesicle solution was drastically reduced upon pumping it through the narrow tube into the S compartment of the SBSR cell and was increased again when the solution front entered the S cuvettes. Since the filling of the S compartment with vesicle solution only took a few minutes, no surface bilayer (multilayer) could probably be restored in the cuvettes. Therefore, completion of the second leaflet of the DPPA/DPPC bilayer is supported to have occurred via direct adsorption from the vesicle solution upon contact of the bulk phase with the DPPA hydrocarbon chains on the ATR plate. The reduction of free surface energy G_s upon coating the hydrophobic surface of the DPPA LB layer by a hydrophilic second layer (POPC, DPPC) may be considered to be the driving force that makes the adsorption process diffusion controlled, at least in the initial phase (cf. Figure 3b,c).

Vesicle disruption upon contact with the immobilized DPPA monolayer is supposed to enhance the free lipid concentration near the interface, thus accelerating the diffusion process to the DPPA surface. A similar adsorption mechanism has been proposed for small unilamellar DPPC vesicles adsorbing at 25 °C to negatively charged barium titanate glass beads.[46]

Schindler has developed a kinetic model to describe the adsorption of lipid molecules to the surface of a vesicle solution,[40] which was complemented by a thermodynamic

(37) Cameron, D. G.; Casal, H. L.; Mantsch, H. H.; van Boulanger, Y.; Smith, I. C. P. *Biophys. J.* **1981**, *35*, 1.

(38) Pink, D. A.; Green, T. J.; Chapman, D. *Biochemistry* **1980**, *19*, 349.

(39) The validity of this estimation may be strengthened by the fact that the two additional methylene groups of the DPPC's choline moiety probably lead to a slight overestimation of the tilt angle since the choline head group is known to be oriented approximately parallel to the bilayer surface (cf. refs 21 and 53). This overestimation could compensate the underestimation of δ caused by a slightly greater extent of hydrocarbon chain segment fluctuations in DPPC than in DPPA.

(40) Schindler, H. *Biochim. Biophys. Acta* **1979**, *555*, 316.

(41) Gershfeld, N. L.; Tajima, K. *Nature* **1979**, *279*, 708.

(42) Cevc, G.; Fenzl, W.; Sigl, L. *Science* **1990**, *249*, 1161.

(43) Ginsberg, L.; Gershfeld, N. L. *Biophys. J.* **1985**, *47*, 211.

(44) Tajima, K.; Gershfeld, N. L. *Biophys. J.* **1985**, *47*, 203.

(45) Wiedmann, T. S.; Cheng, S. M. *J. Colloid Interface Sci.* **1991**, *147*, 531.

(46) Jackson, S.; Reboiras, M. D.; Lyle, I. G.; Jones, M. N. *Faraday Discuss. Chem. Soc.* **1986**, *85*, 291.

treatment by Jähnig.[47] They concluded that a layer of vesicles assembles beneath the air–water interface. This layer maintains vesicle diffusion exchange with the bulk solution and lipid exchange with the surface monolayer. It seems possible that such a mechanism contributes to the adsorption of phospholipids to the immobilized DPPA monolayer, too.

Relevance of the Prepared Bilayers for FTIR-ATR Studies. Kalb et al.[48] demonstrated by means of FRAP (fluorescence recovery after photobleaching) that DPPC and DOPC bilayers supported on oxidized silicon exhibit lateral diffusion coefficients similar to the corresponding multilayers. To the resolution of their experiments, lipids diffused at equal rates in both leaflets. They concluded that there must be a water-filled space between the solid support and the bilayer. This indicates that supported bilayers may be physically very similar to other model membrane systems and justifies their application as model systems for biophysical studies.[48]

Application of supported bilayers in conjunction with quantitative FTIR-ATR spectroscopy provides a particularly promising way to characterize the interaction of substances like peptides or drugs with model membranes. In contrast to other experimental techniques, FTIR-ATR spectroscopy is a nonperturbing technique and permits rather realistic insights into structural and dynamic properties of model membranes in situ, since structural information can be obtained from the side of the ATR plate while the bilayer may interact at the same time with a substrate dissolved in the aqueous medium that can be modified arbitrarily. A particular advantage is the fact that the supported bilayer lies in the most intense part of the evanescent wave, resulting in a maximum of the absorbance ratio of membrane to aqueous phase. With the help of a SBSR setup, the range of reliable FTIR-ATR measurements can be extended easily to the level of submonolayer thickness.

In contrast to ^{2}H-NMR spectroscopy, which cannot be applied to determine order parameters of phospholipids in the gel state because of the lack of motional averaging on the ^{2}H-NMR time scale, IR spectroscopy can be used to derive order parameters in the gel phase as well as in the liquid crystalline phase. Finally, it should be pointed out that FTIR-ATR spectroscopy has the potential to sample directly fast conformational alterations and allows a concomitant measurement or application of membrane surface potentials as well as electric fields.

Conclusions

This paper has demonstrated the reliability of the discussed preparation procedure for supported phospholipid bilayers, using DPPA/POPC and DPPA/DPPC bilayers as examples. From the obtained results it is apparent that these bilayers are very stable in an aqueous environment. Information on the molecular area as well as on the hydrocarbon chain order and an eventual chain tilt in the gel phase could be derived. For these reasons, these prepared bilayers could serve as a useful model system for investigations of biophysical and pharmaceutical phenomena in biological membranes.

Acknowledgment. Support by Sandoz Pharma AG, PE-DDA, Basel; Bruker Analytische Messtechnik, Karlsruhe; Spectrospin AG, Fällenden, and the Kommission zur Förderung der Wissenschaftlichen Forschung (KWF), Bern (Projects No. 1895.5, 2245.1) is kindly acknowledged. U.P.F. is indebted to Prof. R. Hütter, vice president for research of the Swiss Federal Institute of Technology (ETH), for enabling experimental work at the new ETH-Technopark.

Appendix

1. Mean Molecular Order Parameter $\bar{S}_{mol}$. In order to obtain orientational information on the hydrocarbon chains of the prepared membrane leaflets, integrated absorbances of the $\nu_s(CH_2)$ mode were measured with $\parallel$ and $\perp$ polarized light. All methylene groups of a phospholipid molecule contributed to the overall $\nu_s(CH_2)$ integrated absorbance:

$$\int_{band} A_{\parallel}(\tilde{\nu})\, d\tilde{\nu} = a_{\parallel} = \sum_{i=1}^{\nu} a_{i,\parallel} \tag{7a}$$

$$\int_{band} A_{\perp}(\tilde{\nu})\, d\tilde{\nu} = a_{\perp} = \sum_{i=1}^{\nu} a_{i,\perp} \tag{7b}$$

Here, $\tilde{\nu}$ and ν denote wavenumbers in cm^{-1} and the number of methylene groups per molecule, respectively, $a_{\parallel}$ and $a_{\perp}$ ($a_{i,\parallel}$ and $a_{i,\perp}$) are the overall integrated absorbances (integrated absorbances of an individual methylene group) in cm^{-1}.

The integrated absorbance a is proportional to the ensemble average of the square of the scalar product of the electric field $\vec{E}$ of radiation and the transition dipole moment $\vec{M}$. $\vec{M}$ is proportional to the change of the molecular dipole moment $\vec{u}$ with respect to the normal mode displacement q, i.e. $\vec{M} \propto \partial\vec{u}/\partial q$.[49] Thus,

$$a = cd\int \epsilon(\tilde{\nu})\, d\tilde{\nu} \propto \langle(\vec{E}\cdot\vec{M})^2\rangle = |\vec{E}|^2|\vec{M}|^2\langle\cos^2(\vec{E},\vec{M})\rangle \tag{8}$$

where c,d, and $\int\epsilon(\tilde{\nu})\, d\tilde{\nu}$ denote concentration, sample thickness, and integrated molar absorption coefficient, respectively.

Orientational information from eq 8 is stored in the average of the squared direction cosines over the ensemble of the corresponding transition moments, i.e. $\langle m^2\rangle = \sum_{i=1}^{\nu}\langle m_i^2\rangle = \langle\cos^2(\vec{E},\vec{M}_i)\rangle$ for ν equal functional groups per molecule contributing to the absorption process. Since the evanescent wave exhibits electric field components in all directions of the ATR plate-fixed coordinate system, one may calculate integral axial absorbances: a_x, a_y, and a_z, where $a_{\parallel} = a_x + a_z$ and $a_{\perp} = a_y$. Thus, according to eqs 7a,b and 8, one obtains

$$a_{\parallel} \propto |\vec{M}|^2[E_x^{r2}\sum_{i=1}^{\nu}(\langle m_{i,x}^2\rangle) + E_z^{r2}\sum_{i=1}^{\nu}\langle m_{i,z}^2\rangle] \tag{8a}$$

$$a_{\perp} \propto |\vec{M}|^2 E_y^{r^2}\sum_{i=1}^{\nu}\langle m_{i,y}^2\rangle \tag{8b}$$

E_x^r, E_y^r, and E_z^r denote the relative electric field components which decrease exponentially with distance z from the ATR plate according to[11,12,50]

$$E^r(z) = E_0^r e^{-z/d_p} \tag{9}$$

The penetration depth d_p is given by eq 3. In this

(47) Jähnig, F. *Biophys. J.* **1984**, *46*, 687.
(48) Kalb, E.; Frey, S.; Tamm, L. *Biochim. Biophys. Acta* **1992**, *1103*, 307.
(49) Wilson, E. B.; Decius, J. C.; Cross, P. C. *Molecular Vibrations. The Theory of IR and Raman Vibrational Spectra*; McGraw-Hill: New York, 1955.
(50) Harrick, N. J. *Internal Reflection Spectroscopy*; Harrick: Ossining, NY, 1979.

application the bilayer thickness ($d \approx 50$ Å) is small compared with the penetration depth $d_p(\nu_s(CH_2)) \approx 2300$ Å. Thus it follows from eq 9 that $E^r(z = 50\text{ Å})/E^r_0 = 0.978$, justifying the so-called thin layer approximation $E^r(z) \approx E^r_0$ for $0 \le z \le d = 50$ Å. Analytical expressions for the axial electric field components at $z = 0$, E^r_{0x}, E^r_{0y}, and E^r_{0z} result from Fresnel's equations.[50,51] The dichroic ratio R, i.e. the ratio of parallel and perpendicular polarized absorbances (cf. eqs 8a,b), is the relevant experimental parameter for orientation measurements.

$$R = \frac{a_{\parallel}}{a_{\perp}} = \frac{a_x + a_z}{a_y} = \frac{E^{r2}_{0x}\sum_{i=1}^{\nu}\langle m^2_{i,x}\rangle + E^{r2}_{0z}\sum_{i=1}^{\nu}\langle m^2_{i,z}\rangle}{E^{r2}_{0y}\sum_{i=1}^{\nu}\langle m^2_{i,y}\rangle} = \frac{E^{r2}_{0x}\sum_{i=1}^{\nu}\langle \sin^2\alpha_i \cos^2\phi_i\rangle + E^{r2}_{0z}\sum_{i=1}^{\nu}\langle \cos^2\alpha_i\rangle}{E^{r2}_{0y}\sum_{i=1}^{\nu}\langle \sin^2\alpha_i \sin^2\phi_i\rangle} \quad (10)$$

α_i denotes the instantaneous angle between the z-axis (laboratory coordinate system x,y,z; cf. Figures 1 and 6a) and the transition moment $\bar{M}_i$ of the ith segment of ν equal functional groups of the molecule. ϕ_i is the angle between the x-axis and the projection of $\bar{M}$ to the x,y-plane (cf. Figure 6a). ϕ_i is isotropic for uniaxial orientation around z, i.e. the corresponding distribution function $P(\phi_i) = 1$, resulting in

$$\langle \sin^2\alpha_i \cos^2\phi_i\rangle = \langle \sin^2\alpha_i\rangle \int_0^{2\pi} P(\phi_i) \sin^2\phi_i\,(1/2\pi)\,d\phi_i = \frac{1}{2}\langle \sin^2\alpha_i\rangle \quad (10a)$$

Therefore, one obtains from eqs 10 and 10a

$$R = \frac{E^{r2}_{0x}}{E^{r2}_{0y}} + 2\frac{E^{r2}_{0z}}{E^{r2}_{0y}}\frac{\sum_{i=1}^{\nu}\langle \cos^2\alpha_i\rangle}{\nu - \sum_{i=1}^{\nu}\langle \cos^2\alpha_i\rangle} \quad (10b)$$

Equation 10b can be rewritten, substituting the angle α_i for the segmental order parameter of the corresponding CH_2 stretch vibration, $S_{CH_2}(i)$, which characterizes the partial alignment of the transition dipole moment $\bar{M}_i$ with respect to the z-axis. $S_{CH_2}(i)$ is mathematically equivalent to the so-called "bond-order" (or "deuterium-order") parameter S_{CD}, which is used in NMR spectroscopy of phospholipids with selectively deuterated hydrocarbon chains.[52,53]

$$S_{CH_2}(i) = \frac{1}{2}(3\langle \cos^2\alpha_i\rangle - 1) \quad (11)$$

Before $S_{CH_2}(i)$ is introduced into eq 10b, it is transformed into the more widely used *segmental molecular order parameter* $S_{mol}(i)$ of the ith hydrocarbon chain segment (= ith segmental molecular axis).[52,54–56] The vector

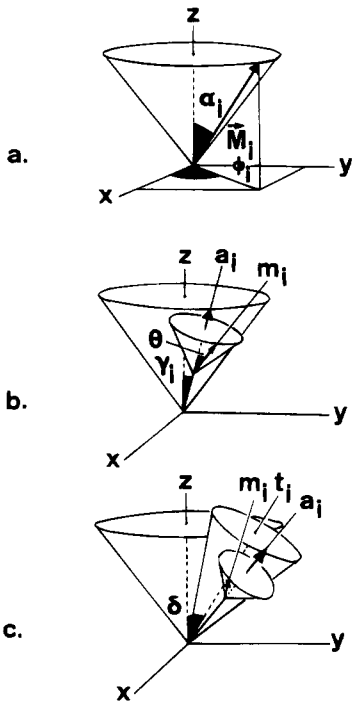

Figure 6. (a) Model for the calculation of $S_{CH_2}(i)$: uniaxial orientation of the ith $\nu_s(CH_2)$ transition dipole moment vector $\bar{M}_i$ around the z-axis; distribution function $P(\phi_i) = 1$. (b) Model for the derivation of $S_{mol}(i)$ in the *liquid crystalline phase*: superposition of two uniaxial distributions. m_i: Instantaneous orientation of the transition dipole moment's unit vector. a_i: instantaneous orientation of the segmental molecular axis. Angles: γ_i, angle between z-axis and a_i; Θ, angle between a_i and m_i. (c) Model for the derivation of $S_{mol}(i)$ in the *gel phase*: superposition of three uniaxial distributions. m_i: instantaneous orientation of the transition dipole moment's unit vector. a_i: instantaneous orientation of the segmental molecular axis. t_i: tilted average orientation of the segmental molecular axis. Angles: δ, tilt angle between z-axis and t_i; γ_i, angle between t_i and a_i; Θ, angle between a_i and m_i.

representing the ith chain segment is orthogonal to the plane spanned by the two C–H bonds of the respective methylene group. $S_{mol}(i)$ measures the distribution of orientations of the ith chain segment instead of the ith transition dipole moment.

For the calculation of $S_{mol}(i)$ from $S_{CH_2}(i)$, a superposition of two uniaxial orientations is assumed (cf. Figure 6b): $\bar{M}_i$ is oriented uniaxially around the segmental molecular axis $\mathbf{a}_i$ with the fixed angle Θ. The segmental molecular axis $\mathbf{a}_i$ exhibits a uniaxial distribution with respect to the z-axis. The angle γ_i between the ith segmental molecular axis and the z-axis is subjected to fluctuations. Thus, the spectroscopically relevant quantity is $\langle \cos^2\gamma_i\rangle$. If the uniaxial distribution of a vector ($\bar{M}_i$) is the result of a superposition of different uniaxially oriented vectors, it follows that the order parameter associated with the first vector can be split up into order-parameter-like factors which refer to the superposed uniaxially distributed vectors; that is,[57]

$$S_{CH_2}(i) = \frac{1}{2}(3\cos^2\Theta - 1)\,S_{mol}(i) \quad (11a)$$

with

(51) Born, M.; Wolf, E. *Principles of Optics*; Pergamon Press: Oxford, 1983.
(52) Seelig, J. *Quart. Rev. Biophys.* **1977**, *10*, 353.
(53) Gennis, R. B. *Biomembranes*; Springer: New York, 1989.
(54) Seelig, J.; Seelig, A. *Annu. Rev. Biophys.* **1980**, *13*, 19.
(55) Bocian, D.; Chan, S. I. *Annu. Rev. Phys. Chem.* **1978**, *29*, 307.
(56) Damodaran, K. V.; Merz, K. M.; Gaber, B. P. *Biochemistry* **1992**, *31*, 7656.
(57) Michl, J.; Thulstrup, E. W. *Spectroscopy with Polarized Light*; VCH: New York, 1986.

$$S_{mol}(i) = \frac{1}{2}(3\langle\cos^2\gamma_i\rangle - 1) \quad (12)$$

This model holds for liquid crystalline systems; it seems reasonable since phospholipids are known to undergo rotations around their long axis above and below the main transition temperature,[58-62] and the average orientation of the hydrocarbon chain segments in the liquid crystalline phase is parallel to the bilayer normal[52] (z-axis).

In the gel phase, however, the latter may not be the case because of a possible hydrocarbon chain tilt. In order to take this into account, the orientational model has to be further extended: it is assumed that a phospholipid monolayer in the gel state is made up of an assembly of crystalline-like mosaics, in which all hydrocarbon chains are tilted with a tilt angle δ and are parallel to each other, and that tilted chains of different mosaics (δ = constant) are distributed statistically in the x/y-plane. This model can be described by the product of three order-parameter-like terms since it can be visualized as a superposition of three uniaxially distributed components: the tilted average molecular axis is distributed uniaxially around the bilayer normal, the instantaneous molecular axis around the mean molecular axis, and the transition dipole moment around the instantaneous molecular axis (cf. Figure 6c):

$$S_{CH_2}(i) = \frac{1}{2}(3\cos^2\Theta - 1)\frac{1}{2}(3\cos^2\delta - 1)\,S_{mol}(i) \quad (13)$$

Equations 11 and 13 can be applied in the liquid crystalline phase and in the gel phase, respectively. In the case of $\delta = 0°$ (liquid crystalline phase or zero chain tilt in the gel phase), eq 13 converts to eq 11. In both cases, $S_{mol}(i)$ is a measure of the extent of the angular fluctuations of the ith segmental molecular axis around its nontilted (or tilted) average orientation. Fluctuations may be due to segmental rotational isomerizations (trans-gauche) or rigid-body type motions of the whole molecule (e.g. off-axis wobble = overall angular fluctuation).[55,63]

Unless selectively deuterated hydrocarbon chains in phospholipid molecules are used, only the *mean orientation* of all segmental molecular axes of the hydrocarbon chains can be determined. Thus, averaging has to be carried out over the ν methylene groups of a phospholipid molecule, leading to the *mean order parameter of the CH_2 stretch vibrations*, $\bar{S}_{CH_2}$,[64] and the *mean molecular order parameter*, $\bar{S}_{mol}$,[65] respectively:[66]

$$\bar{S}_{CH_2} = \frac{1}{\nu}\sum_{i=1}^{\nu} S_{CH_2}(i) = \frac{1}{2}\left[3\frac{1}{\nu}\sum_{i=1}^{\nu}\langle\cos^2\alpha_i\rangle - 1\right] = \frac{1}{4}(3\cos^2\Theta - 1)(3\cos^2\delta - 1)\bar{S}_{mol} \quad (14)$$

with

$$\bar{S}_{mol} = \frac{1}{\nu}\sum_{i=1}^{\nu} S_{mol}(i) \quad (15)$$

A rigid all-trans conformation of nontilted hydrocarbon chains would result in $\bar{S}_{mol} = 1$. For the sake of completeness it has to be noted that not only methylene groups of the hydrocarbon chains contribute to $\bar{S}_{mol}$ but also the two methylene groups of the glycerol moiety. Furthermore, the two methylene groups of the choline head group also have to be considered in the case of phosphatidylcholines, thus resulting in $\bar{S}_{mol} < 1$ even in the all-trans state.

In order to calculate $\bar{S}_{mol}$ from R, the experimentally available quantity $\sum_{i=1}^{\nu}\langle\cos^2\alpha_i\rangle$ is derived from eq 14 and inserted into eq 10b. The resulting equation is then resolved to yield $\bar{S}_{mol}$:

$$\bar{S}_{mol} = \frac{4(E_{0x}^{r2} - RE_{0y}^{r2} + E_{0z}^{r2})}{(3\cos^2\Theta - 1)(3\cos^2\delta - 1)(E_{0x}^{r2} - RE_{0y}^{r2} - 2E_{0z}^{r2})} \quad (16)$$

2. The Surface Concentration Γ of Phospholipids. Calculation of Γ is based on the Lambert–Beer law. Adaptation for ATR technique requires the introduction of a hypothetical thickness d_e ("effective thickness")[50] of the sample which would result in the same absorbance of a given band in a corresponding transmission experiment. For an isotropically oriented sample of thickness d, ranging from z_i to z_f ($d = z_f - z_i$), and ⊥ polarized light, which only results in an electric field component along the y-axis, the effectiveness thickness per internal reflection ($d_{e\perp}^{iso}$) is given by[12]

$$d_{e\perp}^{iso} = \frac{n_{21}d_p}{2\cos\theta}(e^{-2z_i/d_p} - e^{-2z_f/d_p})E_{0y}^{r2} \quad (17)$$

A corresponding expression can be derived for ∥ polarized light in which E_{0y}^{r2} has to be replaced by $(E_{0x}^{r2} + E_{0z}^{r2})$.[11,12] The symbol d_p refers to the attenuation constant of the electric field (eq 3), which declines exponentially in the z-direction ("depth of penetration"),[50] and is calculated by eq 3.[50,67]

The effective thickness of a (partially) oriented sample also depends on the mean orientation of the transition dipole moment, i.e. the mean square of the unit vector component of the transition dipole moment along the y-axis, $\langle m_{i,y}^2\rangle$. Besides, the sum of all $\nu_s(CH_2)$ vibrations in a molecule has to be considered in the case of phospholipids. Thus, $\sum_{i=1}^{\nu}\langle m_{i,y}^2\rangle$ is the relevant quantity to describe the influence of the mean orientation on $d_{e\perp}$. A factor of 3 has to be introduced because $\sum_{i=1}^{\nu}\langle m_{i,y}^2\rangle$ assumes a value of $^1/_3$ in the isotropic case. Consequently, the overall effective thickness $d_{e\perp}$ of (partially) oriented phospholipid molecules with ν methylene groups per molecule can be described by

$$d_{e\perp} = [3\sum_{i=1}^{\nu}\langle m_{i,y}^2\rangle]d_{e\perp}^{iso} \quad (18)$$

Taking into account the assumed uniaxial orientations of all transition dipole moments, $\sum_{i=1}^{\nu}\langle m_{i,y}^2\rangle$ can be substi-

(58) Meier, P.; Ohmes, E.; Kothe, G. *J. Chem. Phys.* **1986**, *85*, 3598.
(59) Mayer, C.; Müller, K.; Weisz, K.; Kothe, G. *LIq. Cryst.* **1988**, *2*, 797.
(60) Tardieu, A.; Luzzati, V.; Reman, F. C. *J. Mol. Biol.* **1973**, *75*, 711.
(61) Gaber, B. P.; Peticolas, W. L. *Biochim. Biophys. Acta* **1977**, *465*, 260.
(62) Davis, J. H. D. *Biophys. J.* **1979**, *27*, 339.
(63) Moser, M.; Marsh, D.; Meier, P.; Wassmer, K. H.; Kothe, G. *Biophys. J.* **1989**, *55*, 111.
(64) In refs 11 and 12 the symbol σ has been used instead of $\bar{S}_{CH_2}$. They are related by the equation $2\bar{S}_{CH_2} = \sigma$.
(65) The symbol S in refs 11 and 12 is equivalent to $\bar{S}_{mol}$ under the assumption $\delta = 0°$.
(66) In a strict treatment, a weighted averaging according to the individual positions of the methylene groups with respect to the declining field of the evanescent wave should be performed. Weighting non-weighted averaging is small under the reported experimental conditions: $E^{r2}(C(15)) \approx 0.94E^{r2}(C(2))$.
(67) n_{31} was used to calculate d_p. Thus, the influence of the lipid membrane on d_p was neglected (thin film approximation).
(68) Taken from ref 10.

tuted for $\bar{S}_{mol}$:

$$\sum_{i=1}^{\nu}\langle m_{i,y}^2\rangle = \frac{1}{2}\sum_{i=1}^{\nu}\langle \sin^2 \alpha_i\rangle = \frac{1}{3}\nu\left[1 - \frac{1}{4}(3\cos^2\Theta - 1)(3\cos^2\delta - 1)\bar{S}_{mol}\right] \quad (19)$$

However, it should be noted that no specific information on the orientational model (ultrastructure of the sample) is required in order to calculate $d_{e\perp}$ and subsequently Γ, because $\bar{S}_{mol}$ in eq 19 can be substituted for the dichroic ratio R by means of eq 16. After this is done, the resulting expression for $d_{e\perp}$ is muliplied by the number of internal reflections and inserted into the Lambert–Beer law. The "concentration" of phospholipids is thereby calculated as $c = \Gamma/d$ (d: thickness of a monolayer), and the resulting equation is resolved to yield Γ:

$$\Gamma = \frac{a_\perp d}{\int \epsilon(\tilde{\nu})\, d\tilde{\nu}\, N d_{e\perp}} = \frac{a_\perp d}{3\int \epsilon(\tilde{\nu})\, d\tilde{\nu}\, N\nu d_{e\perp}^{iso}}\left[2 - \frac{E_{0x}^{r2}}{E_{0z}^{r2}} + R\frac{E_{0y}^{r2}}{E_{0z}^{r2}}\right] \quad (20)$$

$a_\perp$, $\int\epsilon(\tilde{\nu})\, d\tilde{\nu}$, N, ν, and d denote the overall integrated absorbance of $\nu_s(CH_2)$ measured with $\perp$ polarized light (in cm^{-1}), the integrated molar absorption coefficient (ν_s-(CH_2)), the mean number of phospholipid-sensing internal reflections, the number of equal functional groups (methylene groups) per phospholipid molecule, and the thickness of the membrane, which in all cases was a monolayer since different leaflets of the bilayer membrane were analyzed separately.

3. Error Analysis. In all experiments, two diagrams, each containing the time dependence of the $\parallel$ or $\perp$ polarized absorbance ($a_{\parallel,\perp}(t)$), were drawn. Depending on the form of the resulting curves, different functions were used to fit the data points:

$$\hat{a}_{\parallel,\perp}(t) = at + b \quad (21a)$$

$$\hat{a}_{\parallel,\perp}(t) = a + b_1(1 - e^{-c_1 t}) + b_2(1 - e^{-c_2 t}) \quad (21b)$$

$$\hat{a}_{\parallel,\perp}(t) = a - b(1 - e^{ct}) \quad (21c)$$

A constant standard deviation of the fitted values, $s(\hat{a}_{\parallel,\perp}(t))$, was assumed over the whole range of t values and assessed by

$$s(\hat{a}_{\parallel,\perp}(t)) = \left[\frac{1}{n - \nu}\sum_{i=1}^{n}(a_{\parallel,\perp}(t_i) - \hat{a}_{\parallel,\perp}(t_i))^2\right]^{1/2} \quad (22)$$

where n = number of data points, ν = number of variables in the respective fit function ($n - \upsilon$ = degrees of freedom), $a_{\parallel,\perp}(t_i)$ = ith measured absorbance value ($\parallel$ or $\perp$), and $\hat{a}_{\parallel,\perp}(t_i)$ = corresponding fitted absorbance value. $s(\hat{a}_{\parallel,\perp}(t))$ was taken as a measure of the goodness of the fit. Equations 5 and 1 were then applied to compute $\hat{\bar{S}}_{mol}(t)$ and $\hat{\Gamma}(t)$ from $\hat{a}_{\parallel}(t_i)$ and $\hat{a}_\perp(t_i)$. The corresponding standard deviations $s(\hat{\bar{S}}_{mol}(t))$ and $s(\hat{\Gamma}(t))$ were assessed by computing the propagation of errors:

$$s(\hat{\bar{S}}_{mol}(t)) = \left\{\left[s(\hat{a}_{\parallel}(t))\frac{\partial\hat{\bar{S}}_{mol}(t)}{\partial\hat{a}_{\parallel}(t)}\right]^2 + \left[s(\hat{a}_\perp(t))\frac{\partial\hat{\bar{S}}_{mol}(t)}{\partial\hat{a}_\perp(t)}\right]^2\right\}^{1/2} \quad (23)$$

and

$$s(\hat{\Gamma}(t)) = \left\{\left[s(\hat{a}_{\parallel}(t))\frac{\partial\hat{\Gamma}(t)}{\partial\hat{a}_{\parallel}(t)}\right]^2 + \left[s(\hat{a}_\perp(t))\frac{\partial\hat{\Gamma}(t)}{\partial\hat{a}_\perp(t)}\right]^2\right\}^{1/2} \quad (24)$$

The partial derivatives are

$$\frac{\partial\hat{\bar{S}}_{mol}(t)}{\partial\hat{a}_{\parallel}(t)} = \frac{12E_{0y}^{r2}E_{0z}^{r2}}{(3\cos^2\Theta - 1)(3\cos^2\delta - 1)\left[E_{0x}^{r2} - \frac{\hat{a}_{\parallel}(t)}{\hat{a}_\perp(t)}E_{0y}^{r2} - 2E_{0z}^{r2}\right]^2} \times \left[\frac{1}{\hat{a}_\perp(t)}\right] \quad (25a)$$

$$\frac{\partial\hat{\bar{S}}_{mol}(t)}{\partial\hat{a}_\perp(t)} = \frac{12E_{0y}^{r2}E_{0z}^{r2}}{(3\cos^2\Theta - 1)(3\cos^2\delta - 1)\left[E_{0x}^{r2} - \frac{\hat{a}_{\parallel}(t)}{\hat{a}_\perp(t)}E_{0y}^{r2} - 2E_{0z}^{r2}\right]^2} \times \left[-\frac{\hat{a}_{\parallel}(t)}{\hat{a}_\perp(t)^2}\right] \quad (25b)$$

$$\frac{\partial\hat{\Gamma}(t)}{\partial\hat{a}_{\parallel}(t)} = \frac{d}{3\int\epsilon(\tilde{\nu})\, d\tilde{\nu}\, N\nu d_{e\perp}^{iso}}\frac{E_{0y}^{r2}}{E_{0z}^{r2}} \quad (26a)$$

$$\frac{\partial\hat{\Gamma}(t)}{\partial\hat{a}_\perp(t)} = \frac{d}{3\int\epsilon(\tilde{\nu})\, d\tilde{\nu}\, N\nu d_{e\perp}^{iso}}\left[2 - \frac{E_{0x}^{r2}}{E_{0z}^{r2}}\right] \quad (26b)$$

For the assessment of $s(\hat{\bar{S}}_{mol}(t))$, δ was set to zero; i.e., the liquid crystalline phase model was employed since in this case $\hat{\bar{S}}_{mol}(t)$ and $s(\hat{\bar{S}}_{mol}(t))$ can be determined unequivocally. The standard deviation $s(\hat{a}_{mol}(t))$ of the molecular area $\hat{a}_{mol}(t)$ which was determined according to eq 4 was assessed by

$$s(\hat{a}_{mol}(t)) = \frac{10^{16}}{6.022\times10^{23}}\frac{1}{\hat{\Gamma}(t)}s(\hat{\Gamma}(t)) \quad (27)$$